Design and analysis of a linear servo-actuated variable-span morphing wing

Aynul HOSSAIN*,[1], Wei WANG[1], Hailong YUE[1]

*Corresponding author
[1]School of Aerospace Engineering, Shenyang Aerospace University,
37 Daoyi South St, Shenbei, Shenyang, Liaoning, China 110136,
aynul.auvi007@gmail.com*

DOI: 10.13111/2066-8201.2020.12.4.7

Received: 10 September 2020/ Accepted: 05 November 2020/ Published: December 2020

Abstract: *Morphing aircraft are multi-role aircraft that change their external shape substantially to adapt to a changing mission environment during flight. Current interest in morphing vehicles has been increased by advances in smart technologies such as materials, sensors and actuators. These advances have led to a series of breakthroughs in a wide variety of disciplines that, when fully realized for aircraft applications, have the potential to produce large improvements in aircraft safety, affordability, and environmental compatibility. Morphing wing designs include rotating, sliding and inflating based on shape change mechanisms. The current trend in technology development shows that there is lots to improve with regards to aircraft size, flying range and flight performance envelope. There should be a balance between shape change and the penalties in cost, complexity and weight. Final performance of the morphing aircraft depends heavily on how such balances in design, manufacture and morphing mechanism can be achieved. This paper was an attempt to design and perform a further analysis of an efficient variable span wing for aircraft and fixed wing UAVs.*

Key Words: *variable-span, linear actuator, servo, computational fluid dynamics*

1. INTRODUCTION

Morphing technique was introduced by the Wright Brothers who mainly used it for the roll control. They implemented the wing warping method to alter the wing twist condition that consequently ensures the control of the aircraft rolling. The recent advances in adaptive structures and smart materials have created much interest in aircraft applications of these technologies [1]. In particular, one of the areas of high interest of these applications is a morphing wing aircraft, which would be able to change its wing shape over multiple, dissimilar flight segments. Allowing the wing to change its geometry and shape over different mission segments could maximize the efficiency and performance of that aircraft over the entire mission considered [2]. Therefore, it is important to design and analyze a morphing wing. A variable span wing can potentially integrate into a single aircraft the advantages of both designs, making this emerging technology especially attractive for military UAVs [3]. Increasing the wingspan, increases the aspect ratio and wing area, and decreases the span-wise lift distribution for the same lift. Thus, the drag of the wing decreases, and consequently, the range of the vehicle increases. The actuation system was composed of a linear actuator and a small program to control the variable span wing and the sweep actuation were used. The whole

wing consists of two-part main wing, which is a fixed and outer movable wing. The main wing will be attached to the fuselage and the outer movable wing is supported inside the main wing. The outer movable wing (OMW) was designed based on a conventional method.

2. VARIABLE SPAN WING DESIGN

The variable-span wing concept presents a very simple layout, a hollow wing (main wing) inside of which a smaller conventional wing slides (outer movable wing) actuated by a simple electromechanical rack and pinion mechanism. The maximum span length was set to be the same as the original fixed wing 1.29m. For this total span, it was estimated that both the main wing and the outer wing parts would have a 0.29m length, and 0.01m of minimum wing overlapping would allow sufficient wing stiffness in the fully extended configuration. The overall system was designed in CATIA V5 software.

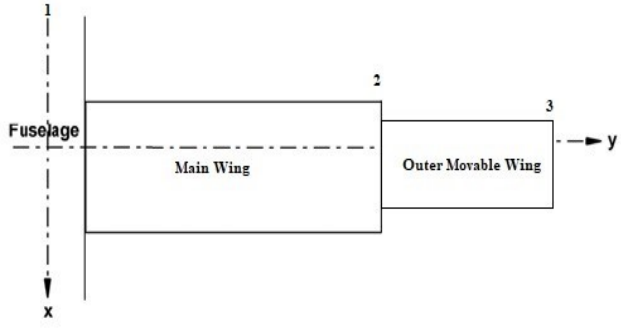

Fig. 1 Wing layout

The main wing (MW) design differs from the outer movable wing (OMW) design. The need to have a hollow wing, in order to allow the OMW to slide inside it, requires a different design approach. In the OMW, the main beam spar conferred the sufficient bending stiffness while the ribs provided the correct wing shape. In main wing, the skin is required to both provide the correct shape and to resist shear loads.

Bending strength was achieved with an unusual main spar configuration made of spar caps embedded in the skin. This allowed a construction from inside out guaranteeing the smallest space between wings, to avoid slacks.

From inside out, the load carrying skin was built, a layer of 0.5mm was incorporated between the rib and layers to allow embedding of the main spar and to give adequate stiffness to the skin since it has no ribs. The complete assembled skin has a 0.5mm thickness, which originated a fairly acceptable small discontinuity between the wings during extended span configuration.

Fig. 2 Assembled wing with linear actuator

The design used in the movable wing is very conventional: the wing is composed of ten 1 mm thick aluminum ribs, a 0.25mm skin and another 1.5mm spar. The main spar on the OMW is of beam type, an unconventional approach in the sense that, despite providing good bending strength, it is also used to align the OMW with the fixed wing. The spar is aluminum alloy with a 1.5mm thickness. Because the main wing had to be hollow, the inner spar is not connected to it. Instead, it is just fixed to the main wing rib and eventually with the fuselage. Both spar were sized to ensure sufficient bending stiffness. The ribs were perforated in order to attach both the I-type beam spar and a rack-guide. The rack used to push/pull the wing is made of aluminum and has a 5mm × 9mm cross-section. It is 0.45m long, which is enough to span the wing length of 0.29m and the stroke needed of 0.30m. To prevent the wing rack from getting stuck when crossing the other wing ribs, rack-guide tube was of aluminum. This guide was assembled with the main wing rib. This actuation system has proven to be adequate to actuate the tip wing.

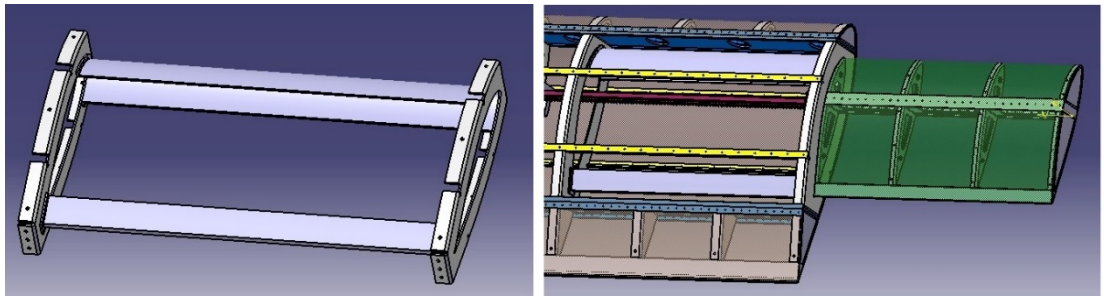

Fig. 3 Extended wing tip section with inner wing support section

In Fig. 3 the wing tip and the inner wing support sections have been shown. The outer movable wing has a support section which will provide housing for the inner wing during the normal condition. Smaller LE section and TE section have been used to provide housing for the inner wing. These smaller sections will be connected between the last rib and 8th rib of the main wing. Summary of the wing specification is shown in Table 1.

Table 1. Wing specification

Design specification	Value
Wing span without extension	1m
Wing span with extension	1.29m
Fully extended wing area (Ansys)	0.68m²
Wing chord	0.28m
Airfoil	Gemini

3. FEA ANALYSIS

The method presented in this paper can be used to design any arbitrary UAV wing having similar aspect ratio. Since we are employing a variable span morphing wing, the area under the lift distribution is equal to the total lift produced by the variable span morphing wing [4]. When the aircraft would undergo the linear extension and increase the wingspan from 1m to 1.29m, it would achieve a higher aspect ratio. Keeping the chord lengths variable, but increasing the span to 0.29 m, we see an increase in the aspect ratio. Additionally, the wing is considered rectangular although the chord of extended section is not equal to the chord of fixed

wing profile. Since the internal structure of the given UAV wing was unknown, the current structure was designed according to the standard wing structural design.

The current structure consists of 3 main components: 9 ribs (7 in fixed wing part with 10cm rib spacing, between last two main wing rib there is 30 cm spacing to accommodate inner wing between them and 4 rib in extended part with 9.45cm spacing), 2 spars at 25% and 72% wing chord, and skin panels. The rib spacing was chosen to have the maximum buckling strength of the panels, while the spars position was chosen to accommodate the maximum torsional stiffness according to the design practices in the wing structural design. The materials and their sectional properties of wing components are presented in Table 2. In addition, mechanical properties of an isotropic material, Aluminium alloy used in the Ansys engineering model has been presented in Table 2.

Table 2. Properties of Aluminum Alloy

Properties	Value
Density	2770 Mpa
Young's Modulus, E	71000 Mpa
Shear Modulus, G	26692 Mpa
Poison's Raito, ν	0.33
Ultimate Strength	310 Mpa
Yield Strength	280 Mpa

3.1 Result and Discussion

After the generation of pressure boundary condition, the wing is fixed at one end and then the static analysis is performed.

The result is given as deformation of the wing in model scale along with Von Mises-stress and strain contour.

The boundary conditions for analyzing the wing conditions are developed by creating pressure load on the lower surfaces of the wing.

Based on Equation 1, the lift is denoted by L; n is the design load factor and W is the weight of the UAV.

Pressure load value of 1 Psi has been estimated. The two different cases shown in Fig. 4 are analyzed one by one, based upon the span change and applied load conditions are given in the following subsections.

$$L = n \times W \tag{1}$$

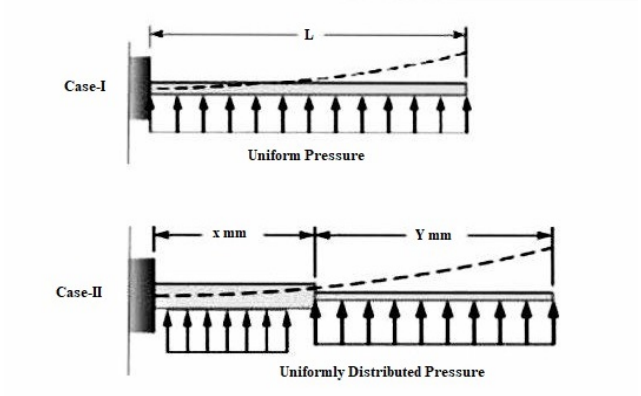

Fig. 4 Applied load condition based on span change

3.1.1 Case I - Without Extension

Figs. 5, 6 and 7, respectively depict the deformation of the un-extended wing along with the stress and strain values. It is clear that the structure is safe enough to take the loads. This structure is safe enough to withstand this particular manoeuvring with enough factor of safety.

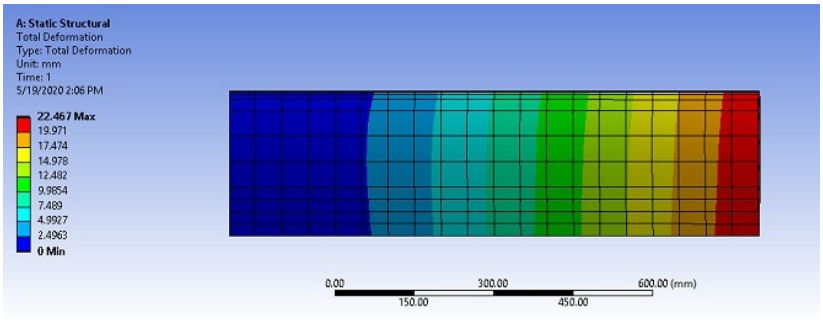

Fig. 5 Total deformation

From Fig. 5, it is very clear that the tip of the wing undergoes maximum deformation and the root region is under tremendous stress, but it is still under control. The maximum deformation value shows 0.022467 m and also the stresses are below the allowable value.

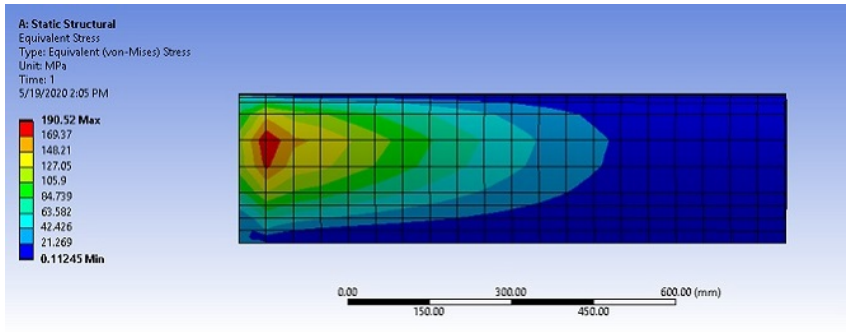

Fig. 6 Equivalent (Von-Mises) stress

From Fig. 6, the equivalent stress has been visualized. The maximum stress seen near the wing root section and near the wing tip stress level is minimum.

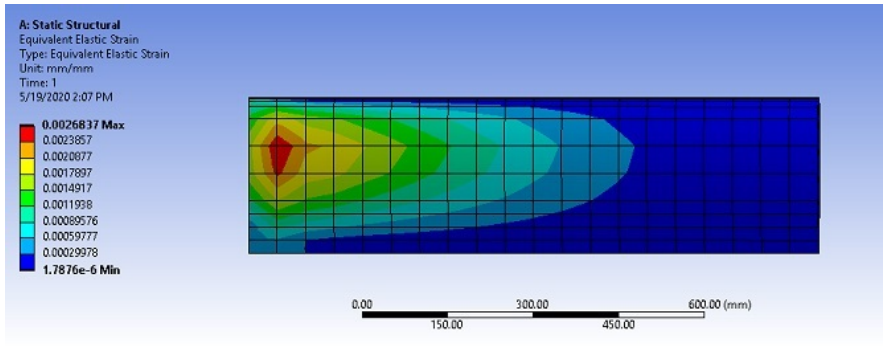

Fig. 7 Equivalent elastic strain

When force is applied, wing is distorted and it is strained. In Fig. 7 we can see how the elastic strain made changes in the wing, where 0.0026837 mm/ mm is the maximum value.

3.1.2 Case II - With Extension

Below three different kind of contours depict the case of static analysis of the span extended wing with uniformly distributed pressure, performed using Ansys static structural workbench.

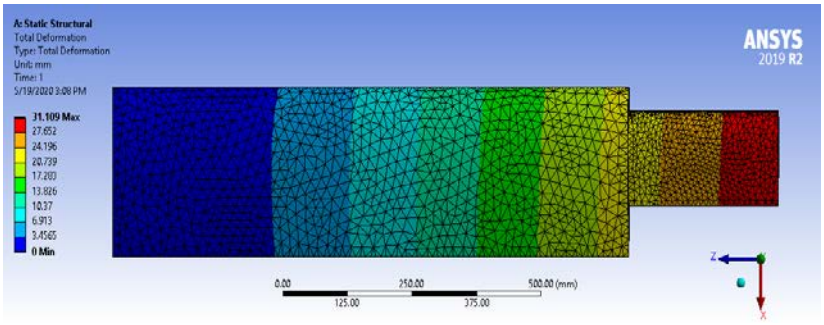

Fig. 8 Total deformation

As expected, it shows that the maximum deflection increases from 0.022467 m for the un-extended wing case to 0.031109 m for the case of telescopic extension of the wing with uniformly distributed pressure throughout the wings.

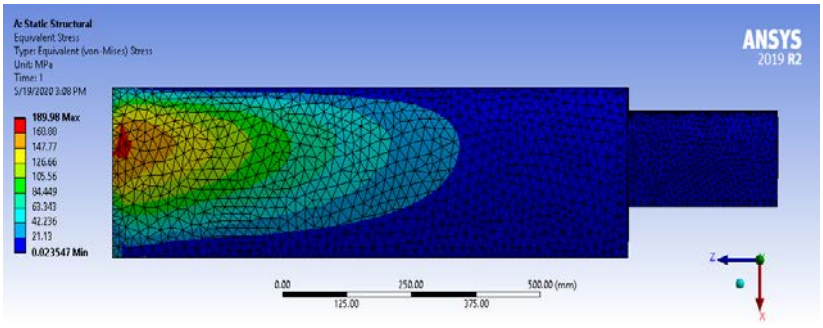

Fig. 9 Equivalent (Von-Mises) stress

From Fig. 9 it is very clear that the root region is under tremendous stress, but it is still under control. The maximum stress value shows 189.98 Mpa and still within the allowable value. It is clear that the structure is safe enough to take the loads.

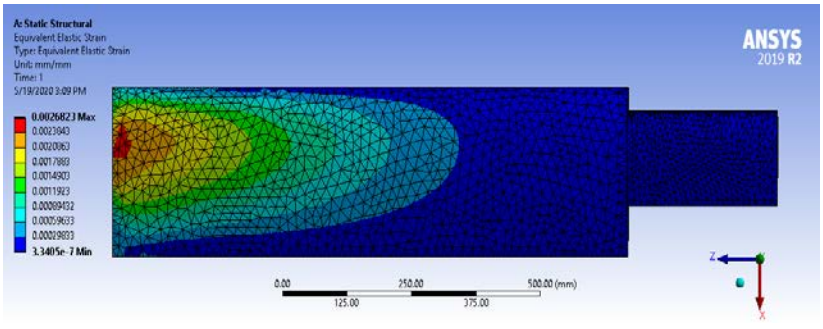

Fig. 10 Equivalent elastic strain

In Fig. 10 we can see that, the equivalent elastic strain for fully extended wing has also the maximum value near the wing root section. Compared to un-extended wing very small changes occurred during extended condition.

4. CFD ANALYSIS

Generally, the aerodynamic performance can be enhanced by changing the aspect ratio of the wing. Variable span morphing wing allows two distinct airfoil sections of the wing to extend its span using another section employing servo gear driven mechanism. The primary airfoil model section is maintained by Gemini with span of 1 meters with full extension to 1.29 meters. Therefore, both two different computational studies are carried out in a span retracted wing and extended wing for 3 degree angles of attack. However, the separation phenomenon and turbulence occurs in the transition regions of wing profile. In addition, endurance is further enhanced for a variable aspect ratio wing because the wing surface area also increases with aspect ratio. By tailoring the wing geometry one can adapt the lift and drag characteristics to a variety of missions. Changing operating conditions and multi-mission requirements, aerospace vehicles are engaged in a number of phases. Usually, the optimization can be achieved by completing mission using fixed geometrical configuration. But this results in the design compromise by affecting the efficiency of other operating phases. For example, an aircraft designed for loiter at low speed, where high speed dashes are preformed between loiter waypoints, might favor a design that maximizes the aspect ratio for the loiter condition, constrained by the requirements of the high speed dash, such as engine thrust, or power, or wing loading [5]. This may lead to lower potential dash speed or shorter range and endurance.

As a result, the adaptive wing is like an avian flight that has capability to adjust its wings to meet multiple flight maneuvers with better performance morphing aircraft bestows the unique ability to increase the efficiency as compared to conventional aircrafts. Various morphing aircraft designs are being investigated by engineers. Approaches of wing morphing include span change [6], wing twist [7], wing sweep change [8], and wing camber [9]. A variable span configuration has ability to meet the requirements of both military and commercial UAVs. Increasing the wingspan, increases the aspect ratio and wing area, and decreases the span-wise lift distribution for the same lift. Thus, the drag of the wing could be decreased, and consequently, the range or endurance of the vehicle increase. The applications of smart materials with their morphing outcomes have also been summarized, and different mechanisms have been listed to achieve multi mission aerospace vehicles [10]. Span morphing technology offers a strategy to modify the wing aspect ratio, and the wing plan form to optimize the flight conditions. Such a study was presented by employing the span morphing on the mission performance of a 25kg UAV [11]. CFD fluent are used to understand the different flow patterns and pressure variations over the various sections of the wing. This study also demonstrates the potential effectiveness of a model meshing on the simulation and emphasizes the sensitivity of the solution outcome to the model solution setup.

4.1 Numerical Strategy and Optimization

To verify the aerodynamic coefficients, the numerical analysis performed is compared to the earlier results found in the literature. The wing area and the aspect ratio of a conventional wing are fixed. For lift augmentation, the lift coefficient can be increased by enlarging the angle of attack of the wing profile.

However, in adaptive wings, same can be achieved by increasing the aspect ratio via changing the area of the wing.

The parameters of total drag (C_D), profile drag (C_{D0}), aspect ratio (AR) and induced drag (C_{Di}) are defined to enhance the aerodynamic efficiency as follows [12].

$$R = \frac{\eta}{C_f}\frac{C_L}{C_D}\ln\left(\frac{W_0}{W_1}\right) \tag{2}$$

$$E = \frac{\eta}{C_f}\frac{C_L^{3/2}}{C_D}\sqrt{2S\rho_\infty}\left(\frac{1}{\sqrt{W_1}} - \frac{1}{\sqrt{W_2}}\right) \tag{3}$$

$$\left(\frac{C_L}{C_D}\right)_{Max} = \frac{(C_{D0}\pi eAR)^{1/2}}{2C_{D0}} \tag{4}$$

$$\left(\frac{C_L^{3/2}}{C_D}\right)_{Max} = \frac{(3C_{D0}\pi eAR)^{3/4}}{4C_{D0}} \tag{5}$$

It is noted that, both the range and the endurance are strongly dependent on equation (4) and (5), respectively. Each of these ratios is dependent on the wing aspect ratio. Thus it is clear that an increase in wing aspect ratio would result in an increase in both range and endurance. In addition, endurance is further enhanced for a variable aspect ratio wing because wing surface area also increases with aspect ratio. By tailoring the wing geometry one can adapt the lift and drag characteristics to a variety of missions.

4.2 Set Up and Solution

After importing the geometry into the Ansys workbench, the mesh is generated and 3D solution domain is set. In order to obtain the optimum solution, two distinct rectangular prisms are created, termed as inner domain and outer domain. The inner domain is much smaller than the outer domain but it comprises ten times more elements than that of the outer domain. The inner domain is nested in such a way that the pressure gradients are higher in the surface of the wing than the far zones.

Pressure based solution is selected with node based gradient option and Spalart-Allmaras model is chosen for viscous condition and air is selected as the fluid with the specific properties (Density = 1.225 [kg/m^3], Viscosity = 1.7894E-05 [kg/ms]). Spalart-Allmaras one-equation model is the most successful eddy viscosity models used today [13] and it has been designed for equilibrium flows where the turbulent time scales are much smaller than the mean flow time scales and react almost instantaneously to changes in the mean strain rate. This assumption is very adequate for flows with no rapid changes in the flow field. However, the major flaw of one and two equation eddy viscosity models is that they do not account for history effects of the Reynolds stresses. Turbulence is produced by the mean strain rate in the flow. Under a non-equilibrium condition, the components of the strain rate tensor are constantly changing.

Thereby, various corrections to eddy viscosity models have been proposed to deal with this, such as the Spalart-Allmaras Model with Rotation and Curvature Correction (SARC) which suppresses turbulent production when the Reynolds stress tensor lags the mean strain rate tensor but does not actually model the physics of the lagging process [14, 15].Some other equations were also added to an existing eddy viscosity model designed to relax the eddy viscosity towards an equilibrium value [16]. Lately, models have been studied which lag the RST instead of the eddy viscosity, called as the lagRST model developed [17], and was commenced for skin friction and separation predictions. The Spalart-Allmaras (SA) turbulence model and the Menter k-ω shear-stress transport (SST) turbulence model have been widely-used and trusted models for Reynolds averaged Navier-Stokes (RANS) computations of aerodynamic flows for well over a decade [18, 19]. Earlier, many CFD simulations in three dimensions have been investigated for high lift devices using these models, which include

those of Mathias et al. [20] who studied a simple wing with half-span flap. There are many advantages in considering CFD. The theoretical development of the computational sciences focuses on the construction and solution of the governing equations and the study of various approximations to these equations. CFD complements experimental and analytical approaches by providing an alternative cost-effective means of simulating real fluid flows. Particularly, CFD substantially reduces lead times and costs in designs and production compared to experimental-based approach and offers the ability to solve a range of complicated flow problems where the analytical approach is lacking.

4.3 Model Meshing

A three-dimensional geometric model was developed using CATIA V5 and later imported in Ansys fluent for meshing as in Fig. 11. In order to facilitate the solution, the geometric model should be small and simple in design, but must meet all the requirements of each individual part with maximum accuracy. The smaller model provides checked meshing nodes and the mesh grid quantity will directly impact the solution duration. It is noted that the model of the wing is Gemini profile with chord of 0.28 m and full span of 1.29 m, respectively. The extended model observed will be employed after validating the solution for the Gemini airfoil.

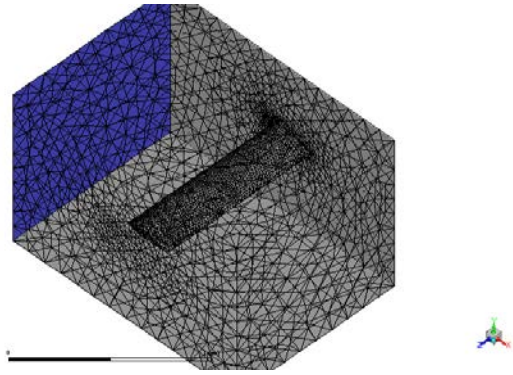

Fig. 11 Mesh generation of un-extended wing

The model meshing is the most significant and refined process in CFD simulations. The characteristics of meshing are determined by the technique of the meshing. Innumerous grid cells or elements are created in the meshing process which is required to solve all the desired fluid flow equations. The grid size has a significant impact on the computational time which in turn influences the cost of simulations. The grid will also have a significant effect on the convergence speed and solution accuracy. In case of successful computations of turbulent flows in a wing model, some boundary layer considerations are also required in mesh generation. Due to strong interaction of the mean flow and turbulence, the numerical results of the turbulent flow show more sensitivity towards the grid dependency than laminar flow. The grouping of the grid in the direction normal to the surface solves the boundary layer solution, with the spacing of the first grid point off the wall to be well within the laminar sub-layer of the boundary layer. Therefore, hexagonal or prism elements are employed to discrete boundary layers to preserve the accuracy in the wall normal direction for highly stretched viscous grid. Aerodynamic coefficients being the focus of investigations in an aerodynamic wing, the surface gridding strategy with defined element size should be taken based on the local chord length. A size of 0.1% of local chord length at leading and trailing edge is good enough to resolve the flow physics and about 5% of the local chord length is good enough to resolve the flow phenomenon along the span-wise direction.

4.4 Result and Discussion

Initially, the investigation of wing without span change having Gemini airfoil is performed. The results are presented as static pressure contour plots of upper and lower surfaces shown below. 0.1 Psi has been estimated. The two different cases shown in the next section are analyzed one by one, based upon the span change and applied load conditions are given in the following subsections.

4.4.1 Case I - Without Extension

The wing profile without span extension. The results are presented as static pressure contour plots for upper and lower surface as seen in Fig. 12 below. The pattern for the pressure change can be found in the wing with trailing edge and leading edge having a higher pressure value.

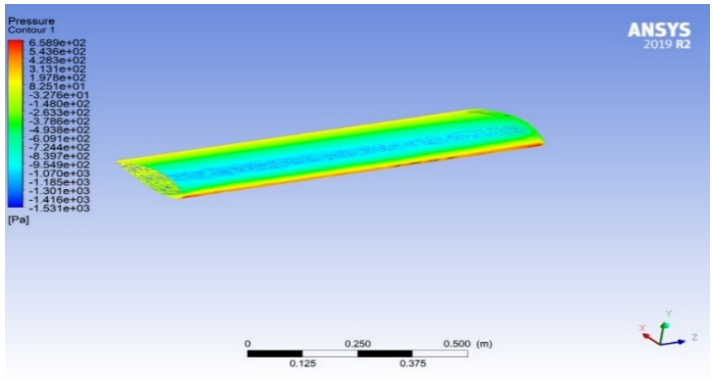

Fig. 12 Pressure distribution of un-extended wing profile

It is clear from the figures above that, the leading edge has the highest pressure value in the wing. Also the chord-wise and span-wise pressure distribution is clearly seen in the Figure above.

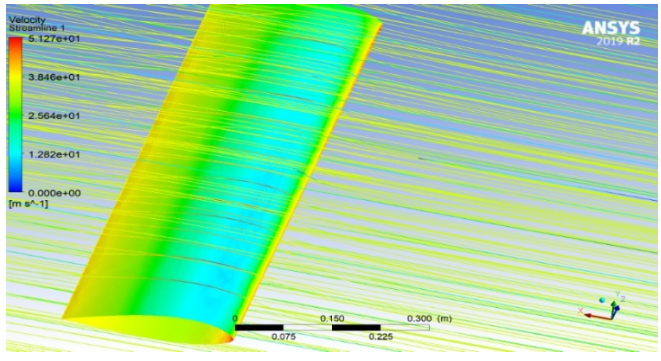

Fig. 13 Velocity streamline of un-extended wing profile

Also the streamline is shown in Fig. 13. Streamlines are curves that are everywhere tangent to the velocity vector. Streamlines are a very good representation of the velocity field. The animation shows streamlines for a steady state 3d flow. For 3d flow fields, instead of streamlines one usually visualizes streaklines or pathlines, which for steady flow are the same. Calculating the stream function and isolines is a more efficient way to calculate streamlines than by integrating particle tracks. So, we can easily understand the properties of velocity streamline flow in upper and lower section of the wing.

4.4.2 Case II - With Extension

The second model is the wing profile with extended span. The results are presented as static pressure contour plots for upper and lower surface, as seen in Fig. 14. The same pattern for the pressure change is found in the leading edge having a higher pressure value. The pressure variation is observed mostly in the extended wing section of the wing model. It is because during the extension, the flow in the wing tip coming from the lower surface disturbs the upper surface.

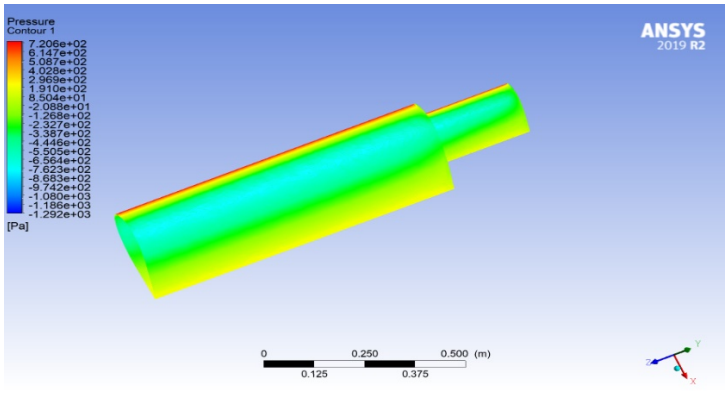

Fig. 14 Pressure distribution of extended wing profile

The velocity stream lines are also presented in Fig. 15 to observe the flow patterns more accurately. It is seen that, the extended wing section of the span adaptive model has denser stream lines. This may be attributed to the vortex generation phenomenon at the place where the wing section starts to extend and form a transition region for the flow. The streamlines behind the wings remain parallel to the free stream.

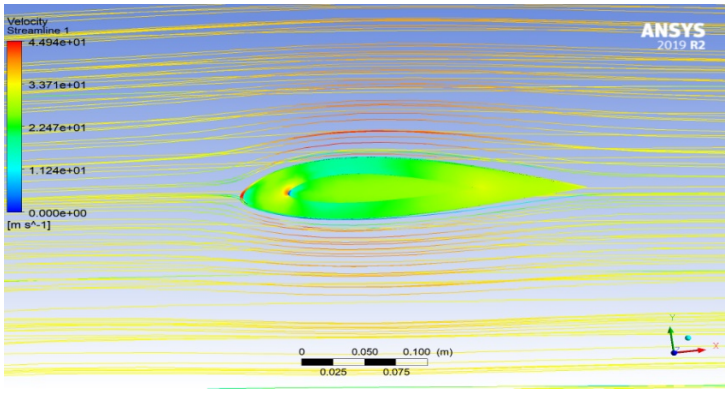

Fig. 15 Velocity streamline of un-extended wing profile

5. CONCLUSIONS

The purpose of this project was to assess the advantages of a variable span wing over a fixed wing platform. First, the design requirements and constraints were addressed. A systems engineering approach was adopted as the main design methodology to account for potential design changes. The morphing UAV wing model as per the design considerations is developed in CATIA V5 and the model is imported into Ansys Static Structural, Fluent and subjected to two different loading.

The loading is calculated according to the aerodynamic lift load analysis by considering that various design factors and the deflection over have been estimated. As seen in the results, the wing is severely affected by the loads on extended part, and the deflection is maximum at the tip of extended section. Moreover, the moment loading applied in one case shows the deflection increases further by the moment force. Also, the stress and strain values increased at the hinged joints between the two wing sections. Von-misses stress is calculated in order to know the maximum stress levels and minimum stress levels on the wing. Their differences are shown clearly with the contour stress levels. The deflection and stress levels are shown from minimum to maximum in the color contours. Their values are given side by side. The wing structure has been optimally analyzed which satisfies the strength and stability criteria. According to the result validation and the analysis being done we can conclude that, the developed method can fulfill any design requirement to develop an efficient morphing wing.

REFERENCES

[1] J. Valasek, *Morphing aerospace vehicles and structures*, John Wiley & Sons Ltd, 2012, West Sussex, United Kingdom.

[2] A. Concilio, I. Dimino, L. Lecce, R. Pecora, *Morphing wing technologies, large commercial aircraft and civil helicopters*, Butterworth-Heinemann, Oxford, United Kingdom, 2017.

[3] T. A. Weisshaar, *Morphing aircraft technology – new shapes for aircraft design, Multifunctional Structures/ Integration of Sensors and Antennas*, Meeting Proceedings RTO-MP-AVT-141, 2006.

[4] R. D. Vocke, C. S. Kothera, B. K. S. Woods and N. M. Wereley, Development and testing of a span-extending morphing wing, *Journal of Intelligent Material Systems and Structures*, vol. **22**, no. 9, pp. 879-890, 2011.

[5] P. Santos, J. Sousa and P. Gamboa, Variable-span wing development for improved flight performance, *Journal of Intelligent Material Systems and Structures*, vol. **28**, no. 8, pp. 961-978, 2017.

[6] C. S. Beaverstock, R. M. Ajaj, M. I. Friswell, R. De Breuker and N. P. M. Werter, *Optimising mission performance for a morphing MAV*, Proceedings of the Ankara International Aerospace Conference, Turkey, 2013.

[7] R. Pecora, F. Amoroso and L. Lecce, Effectiveness of wing twist morphing in roll control, *Journal of Aircraft*, vol. **49**, no. 6, pp. 1666-1674, 2012.

[8] N. Prabhakar, R. J. Prazenica and S. Gudmundsson, Design and dynamic analysis of a variable-sweep, variable-span morphing UAV, *2015 IEEE Aerospace Conference*, United States.

[9] C. Evans, M. Harmer, O. Marks, S. Tiley, T. Willis, A. Bouferrouk and Y. Ya, *Development and testing of a variable camber morphing wing mechanism*, 2nd International Symposium on Sustainable Aviation, Turkey, 2016.

[10] M. Bashir, P. Rajendran, T. F. Ng and L. Wang, Outline for mission-based morphing evaluation with smart material technology, *International Journal of Applied Engineering Research*, vol. **11**, no. 6, pp. 4012-4016, 2016.

[11] C. S. Beaverstock, B. K. S. Woods, J. H. M. Fincham and M. I. Friswell, Performance comparison between optimized camber and span for a morphing wing, *Aerospace*, vol. **2**, no. 3, pp. 524-554, 2015.

[12] J. D. Anderson Jr, *Introduction to Flight, Mc Graw-Hill Company*, New York, United States, 2015.

[13] A. M. Rosen, *Turbulence Modeling for Subsonic Separated Flows Over 2-D Airfoils and 3-D Wings*, Ph.D. Thesis, Purdue University, 2013, Indiana, United States.

[14] P. Spalart and M. Shur, On the sensitization of turbulence models to rotation and curvature, *Aerospace Science and Technology*, vol. **1**, no. 5, pp. 297-302, 1997.

[15] M. L. Shur, Al. Et, M. Strelets and A. K. Travin, Turbulence modeling in rotating and curved channels: assessing the Spalart-Shur correction, *AIAA Journal*, vol. **38**, no. 5, pp. 784-792, 2000.

[16] M. E. Olsen, R. P. Lillard and T. J. Coakley, *The lag model applied to high speed flows*, AIAA Paper, 2005.

[17] P. R. Lillard, *Turbulence modeling for shock wave/turbulent boundary layer interactions*, Ph.D. Thesis, Princeton University, 2011, NJ, United States.

[18] P. R. Spalart and S. R. Allmaras, A one equation turbulence model for aerodynamic flows, *AIAA Journal*,1992.

[19] L. C. Rumsey and P. R. Spalart, Turbulence model behavior in low Reynolds number regions of aerodynamic flow fields, *AIAA Journal*, vol. **47**, no. 4, pp. 982-993, 2009.

[20] D. L. Mathias, K. R. Roth, J. C. Ross, S. E. Rogers and R. M. Cummings, Navier-Stokes analysis of the flow about a flap edge, *Journal of Aircraft*, vol. **35**, no. 6, pp. 833-838, 2012.